Earthquakes and Structures, *Vol. 17, No. 4 (2019) 337-354*
DOI: https://doi.org/10.12989/eas.2019.17.4.337

Experimental investigations and FE simulation of exterior BCJs retrofitted with CFRP fabric

Abdulsamee M. Halahla*[1], Muhammad K. Rahman[2a], Ali H. Al-Gadhib[3b], Mohammed A. Al-Osta[3c] and Mohammed H. Baluch[3d]

[1]*Civil Engineering Department, Fahad Bin Sultan University, Tabuk, 71454, Saudi Arabia*
[2]*Center for Engineering Research, Research Institute, King Fahd University of Petroleum & Minerals, Dhahran 31261, Saudi Arabia*
[3]*Civil & Environmental Engineering Department, King Fahd University of Petroleum & Minerals, Dhahran 31261, Saudi Arabia*

(*Received May 18, 2019, Revised July 18, 2019, Accepted August 30, 2019*)

Abstract. This paper presents the results of experimental and numerical studies conducted to investigate the behavior of exterior reinforced concrete beam column joints (BCJ) strengthened by using carbon fiber reinforced polymer (CFRP) sheets. Twelve reinforced concrete beam-column joints (BCJ) were tested in an experimental program by simulating the joints in seismically deficient old buildings. One group of BCJs was designed to fail in flexure at the BCJ interface, and the second group was designed to ensure joint shear failure. One specimen in each set was -retrofitted with CFRP sheet wrapped diagonally around the joint. The specimens were subjected to both monotonic and cyclic loading up to failure. 3D finite element simulation of the BCJs tested in the experimental program was carried out using the software ABAQUS, adopting the damage plasticity model (CDP) for concrete. The experimental results showed that retrofitting of the shear deficient, BCJs by CFRP sheets enhanced the strength and ductility and the failure mode changed from shear failure in the joints to the desired flexural failure in the beam segment. The FE simulation of BCJs showed a good agreement with the experimental results, which indicated that the CDP model could be used to model the problems of the monotonic and cyclic loading of beam-column reinforced concrete joints.

Keywords: exterior beam-column joint; retrofitting; monotonic test; cyclic test; CFRP; finite element model; damage plasticity model

1. Introduction

A large stock of reinforced concrete (RC) buildings, which were designed based on old seismic codes and in many cases for gravity loads, exists worldwide. These buildings, which have shear deficient beam column joints (BCJs) are vulnerable to failure in a seismic event as the deformation ability of the adjoining beams are limited (Bruneau *et al.* 1996, Saatcioglu *et al.* 2001). The exterior and corner BCJs joints are most susceptible to failure due to confinement by beams on only two faces. The deficiency in the BCJs arises from a lack of stirrups in the joint region and the low quality of concrete used in the construction. When subjected to seismic excitations there is a progressive deterioration in both the strength and stiffness of the BCJs (De Vita *et al.* 2017). Recent earthquakes in Turkey, Italy and several other countries have exhibited shear failure in BCJs leading to the collapse of a building (Celik and Ellingwood 2008).

Investigations into the seismic retrofitting of deficient BCJs have been reported on, both experimentally and numerically, in the literature using various techniques including concrete and steel jacketing. Engineered cementitious composites in beam column joints have also been investigated (Liang and Lu 2018). Strengthening of BCJs using innovative ultra-high strength concrete jacketing with steel fibers (Tsonos 2014) enhances the shear capacity and ductility of the joints substantially. Karayannis and Chalioris (2013) investigated 10 damaged exterior BCJs retrofitted by a thin jacket made of high strength, rapid hardening, flowable mortar reinforced with small dia steel bars. The thin jacket was found to be very effective in restoring the original strength and energy dissipation capacity of the damaged BCJs. In recent years, however, carbon fiber and glass fiber reinforced polymer (CFRP and GFRP) sheets have become a popular choice for seismic retrofit in view of the host of advantages they offer in terms of application and durability. Bidirectional GFRP sheets applied to joints resulted in an increase in the shear strength of the joint and improved the bond of the longitudinal steel rebars in beams (El-Amoury and Ghobarah 2002). Experimental investigations performed on deficient BCJs (Ghobarah and El-Amoury 2005)

*Corresponding author, Assistant Professor
E-mail: ahalahla@fbsu.edu.sa
[a]Associate Professor
E-mail: mkrahman@kfupm.edu.sa
[b]Associate Professor
E-mail: agadhib@kfupm.edu.sa
[c]Assistant Professor
E-mail: malosta@kfupm.edu.sa
[d]Professor
E-mail: mohsain.baluch@gmail.com

ISSN: 2092-7614 (Print), 2092-7622 (Online)

strengthened by using a combination of GFRP and steel members demonstrated the transformation of the brittle shear failure of joints to a ductile mode of failure. Tsonos (2004a) conducted experimental investigations on RC and high-strength fiber jacketing of exterior BCJs prior to load application and after being subjected to cycling loading. The results showed that the RC jacketing of BCJs prior to load application was more effective in enhancing the strength and stiffness of the joint, while in repaired specimens both systems were equally effective. A detailed experimental study was carried out by Antonopoulos and Triantafillou (2003) on 18 seismically deficient BCJs. The parameters investigated included shear reinforcement in the joint, the level of axial load in the column, and the amount, geometry, and type of FRP reinforcement (sheets or laminates) in the beam and column members. Del Vecchio *et al.* (2014) experimentally studied the behavior of full-scale RC corner joints strengthened with different carbon fiber reinforced polymer (CFRP) layouts employing both uniaxial and quadriaxial sheets. Realfonzo and Napoli (2009) investigated the behavior of RC BCJs under combined axial load and bending moment. There was no shear reinforcement in the joint region and the joints were strengthened with CFRP, which was coupled with steel members or steel rods. Bedirhanoglu *et al.* (2010) studied the behavior of eight full-scale RC joints with plain bars and low-strength concrete and no transverse reinforcement in the joint cores, which were retrofitted using CFRP, under cyclic loading.

In order to enhance the shear capacity of the BCJs, shear stirrups are now mandatory in the joints as per various codes. Several researchers have investigated the inclined bars or the X-bars in the joint region to enhance the shear capacity and ductility of the joints (Bakir 2003, Bindhu *et al.* 2008, Chalioris and Bantilas 2017, Lu *et al.* 2012). Tsonos (2004b) investigated the effect of simultaneous axial load and load-deflection experimentally and theoretically on 12 exterior BCJs with inclined bars in the joint region. The inclined bars were found to be effective in reducing the damage, which results from increasing axial load compared to the conventional reinforced joints with shear stirrups. Chalioris *et al.* (2008) showed experimentally that X-bars in the joint region without shear stirrups resulted in enhanced hysteretic response. Analytical equations for predicting the response of BCJs with X-bars have also been proposed (Bakir 2003, Bindhu *et al.* 2008) based on experimental investigations. Chalioris and Bantilas (2017) have proposed analytical model and failure criteria for BCJs with X-bars in the joint region. The enhanced performance of BCJs with X-bars in the joint region shows that external application of near surface mounted X-bars in the joint region and the X-shape configuration of the FPR sheets in the joint region could be a preferred mode of application.

Le-Trung *et al.* (2010) investigated the behavior of exterior BCJs (1/3 scale), retrofitted by CFRP sheets using various types of configuration. The optimal configuration for retrofitting the BCJs for improving the load resisting capacity and ductility was suggested. The x-shaped pattern of 2-layer CFRP sheets wrapped on the joint and the column was determined to be the optimal configuration in terms of ductility and strength. Karayannis and Sirkelis (2008) investigated 12 exterior BCJs sub-assemblages repaired and/or strengthened using a combination of epoxy resin injection and CFRP sheets under cyclic loading reporting a significant enhancement in load carrying capacity energy absorption and ductility. The seismic behavior of six 2/3 scaled exterior Knee (2 Nos.), Tee (2 Nos.) and two interior cruciform RC-BCJs designed without seismic load detailing was investigated by Pampanin *et al.* (2002). Smooth bars were used in the BCJs with inadequate anchorage. Slippage of the bars and stress concentration at the hooked ends resulted in the formation of a concrete wedge at the joints. Ravi and Arulraj (2010) conducted an experimental work to study the effect of development length in retrofitted reinforced concrete beam-column joints with GFRP and CFRP. The load carrying capacity and energy absorption capacity of the BCJs increased by 14.5% and 10% respectively with an increase in the development length. Deficiently detailed corner BCJs retrofitted using CFRP sheets were investigated by Alsayed *et al*. (2010). The test results indicated improvements in shear capacity, ductility of retrofitted specimens and slower stiffness degradation after FRP retrofit. Sasmal *et al.* (2011) investigated the aspects of repair and retrofitting techniques adopted for RC BCJ specimen under cyclic loading. Specimens were devoid of any seismic detailing at the joints and were repaired by CFRP sheet wraps and steel plate with epoxy mortar and grout using low viscous polymer. The results showed that the cumulative energy dissipation for the retrofitted specimen was almost 25% more than that of the control specimen.

Based on the experimental investigations, several authors have proposed analytical procedures for computing the load capacity of existing deficient RC BCJs and enhancements in the load capacity after retrofitting with CFRP/GFRP sheets (Akguzel and Pampanin 2012, Del Vecchio *et al.* 2014). The numerical simulation of RC BCJs tested experimentally by simulating seismic loads has been carried out by several researchers using commercial finite element software including ABAQUS, ANSYS, DIANA etc. (Alhaddad *et al*. 2012, Li and Kulkarni 2010, Niroomandi *et al.* 2010). Supaviriyakit *et al.* (2008) performed a nonlinear FE analysis of RC BCJs without any shear reinforcement in the joint under reversed cyclic load. Ahmed *et al.* (2014) used the software DIANA to carry out nonlinear FE analysis of exterior BCJs constructed using low concrete compressive strength. Ibrahim and Sh Mahmood (2009) used FE in an ANSYS environment to compare the response of six experimentally tested reinforced concrete beams externally reinforced with fiber reinforced polymer (FRP) laminates. The smeared cracking approach for concrete and 3D layered elements for the FRP composites were used in this model. Khan *et al.* (2018) evaluated the behavior of shear-deficient BCJs repaired by using ultra-high-performance fiber reinforced concrete (UHPFRC). It was reported that strengthening BCJs with UHPFRC enhanced the behavior of specimens in terms of shear capacity, deformation capacity, stiffness characteristics and the energy dissipation capacity of BCJs, as compared to the control one. Mobin *et al.* (2016) investigated the performance of the cyclic behavior of interior reinforced concrete BCJs with self-consolidating concrete and Carmo *et al.* (2017) investigated BCJs with

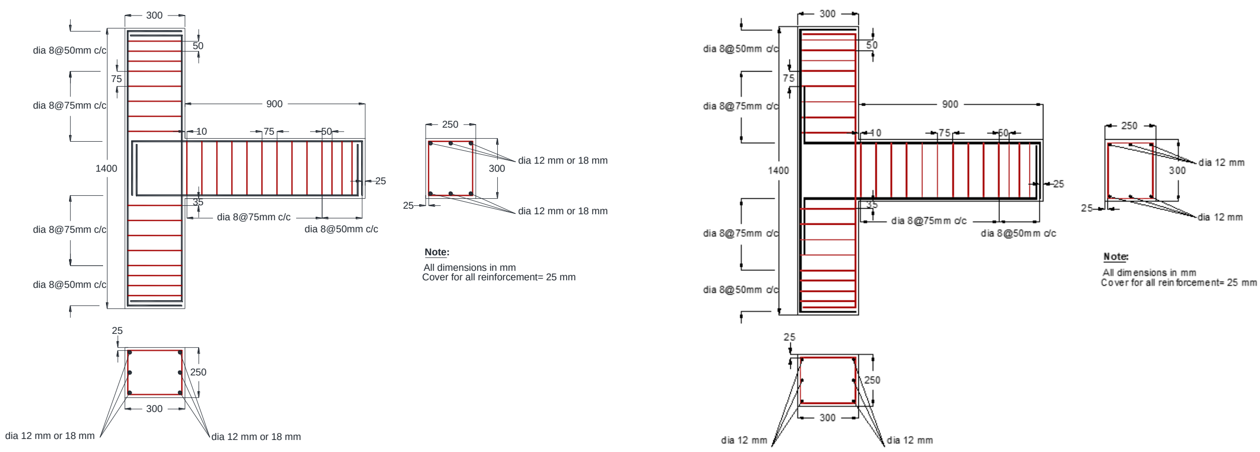

(a) BCJs-12 mm or 18 mm bent in (b) BCJ-12 mm-bent up

Fig. 1 Geometry and steel reinforcement configuration for reinforced concrete specimens

Table 1 Specimen details

Specimens ID	Joint Region Strengthening with CFRP	Main Steel Reinforcement of beam (Top and bottom) [mm]	Reinforcement ratio	Joint Region Ties	Test Method
BCJ-18MM-Bent In	No	6 Φ18	0.0118	No	Monotonic
BCJ-12MM-Bent Up		6 Φ12	0.0052		
BCJ-12MM-Bent In					
BCJ-18MM-Bent In - CFRP	Yes	6 Φ18	0.0118		
BCJ-12MM-Bent Up - CFRP		6 Φ12	0.0052		
BCJ-12MM-Bent In - CFRP					
BCJ-18MM-Bent In	No	6 Φ18	0.0118		Cyclic
BCJ-12MM-Bent Up		6 Φ12	0.0052		
BCJ-12MM-Bent In					
BCJ-18MM-Bent In - CFRP	Yes	6 Φ18	0.0118		
BCJ-12MM-Bent Up - CFRP		6 Φ12	0.0052		
BCJ-12MM-Bent In - CFRP					

lightweight aggregate concrete and different reinforcement ratios. Al-Osta *et al.* (2017) investigated, experimentally and numerically, the performance of BCJs where the concrete in the joint was replaced by steel fiber reinforced concrete (SFRC) and by UHPFRC. The results indicated that the use of both SFRC and UHPC in the joint instead of the normal concrete for the BCJs enhanced the shear capacity of the hybrid BCJs. Al-Osta *et al*. (2018) studied experimentally and numerically the effect of axial load levels of columns on the behavior of BCJs under both monotonic and cyclic loading. The results showed that increasing the axial load of columns enhances the shear capacity of the BCJ and reduces its ductility. Research on improvement of seismic response of BCJs continues to be an active area and several groups around the world are looking into various innovative techniques using innovative materials and technologies for this purpose. Chalioris *et al.* (2018) have shown that FRP ropes embedded at the center of the deep beams, significantly enhanced the shear strength of deep beams and this technique could be considered for the BCJs. Use of continuous rectangular spiral reinforcement in shear critical beams has shown to improve the post-peak deformation ductility (Karayannis and Chalioris 2013).

This paper presents the results of experimental and numerical studies conducted to investigate the behavior of 1/3 full-scale, deficient reinforced concrete BCJs under cyclic and monotonic loading. In this study, no transverse reinforcement was used in the joint and the longitudinal steel bars in the beam were bent in and bent up in the column. Some specimens were retrofitted with CFRP sheet wrapped diagonally around the joint. In addition, a 3-D finite element model for the retrofired BCJ with CFRP sheets was developed by using the concrete damage plasticity model (CDP).

2. Experimental program

2.1 Test specimens and geometry

Twelve reinforced concrete exterior BCJs fabricated on 1/3rd scale were tested in the experimental program. The specimens were tested under monotonic and cyclic loading. All specimens have identical geometry. These specimens were designed with no transverse shear reinforcement in the joint region. The beams have a cross section dimension of 250 mm width and 300 mm depth, whereas, the columns are

Table 2 Properties of concrete

Cylinder	Cylindrical Compressive Strength (f'_c) (MPa)
1	30.02
2	30.88
3	30.26
Mean	30.71

Table 3 Properties of the reinforcing steel bars

Steel Rebar Dia.	Yield strength (f_y) (MPa)	Ultimate strength (f_u) (MPa)	Hardening Ratio (f_u/f_y)
Φ8	437	575	1.31
Φ12	560	624	1.25
Φ18	579	678	1.32

300 mm wide and 250 mm in depth as shown in Fig. 1. All columns are reinforced with 6-25 mm dia bars. The beams have two types of reinforcement: reinforced by 6-12 mm dia and 6-18 mm dia bars. The beam specimen "BCJ-12 mm-Bent up" has longitudinal bars, which are bent up in the columns, while the specimen "BCJ-12 mm Bent in" has longitudinal reinforcement bent as regular hooks. The beam specimen with 18 mm dia bars are bent-in and called "BCJ-18 mm Bent in". The cantilever span of the beam is 900 mm and the total height of the column is 1400 mm. The shear reinforcement in the beams and columns are 8 mm diameter 2-legged closed stirrups spaced at 75 mm c/c to avoid shear failure, except for the ends where the spacing is reduced to 50 mm c/c to ensure adequate strength at the points of load application. The longitudinal reinforcement in the column runs through the joint from the top of the column to the bottom. Table 1 shows the details of all specimens. Based on standard analytical procedures and the mechanical properties of concrete and steel, the expected failure mode in beams with 12 mm dia bars is caused by the yielding of the steel reinforcement in the beam without joint shear failure and for beams with 18 mm dia bars by joint shear failure. Three non-retrofitted specimens and three CFRP retrofitted specimens were tested under monotonic loading, and a second group of the above specimens was tested under cyclic loading.

2.2 Material properties of steel, concrete and CFRP

The concrete compressive strength, fc' was evaluated based on 75×150 mm cylinder samples of the concrete used in the BCJs in accordance with ASTM C39. The compressive strength values after 28 days for each sample are shown in Table 2 where the average value of fc' is 30.7 MPa. The modulus of elasticity of concrete was 26 GPa. The split tensile strength tests were conducted on a 75×150 mm cylinder in accordance with ASTM C496. The average value of tensile strength is 2.2 MPa.

Tensile strength tests were carried out on the reinforcing bars used in the BCJs. Tests were carried out on three specimens for each of the three bar diameters (8 mm, 12 mm and 18 mm). The mean values of yield strength (f_y), ultimate strength (f_u) and hardening ratio (f_u/f_y) are shown in Table 3. The mechanical properties of CFRP sheets used in the experimental program are shown in Table 4. These

Table 4 Proprieties of CFRP sheet (Sika Construction Chemicals 2006)

Thickness (mm)	Young's Modulus E_1 (MPa)	Young's Modulus E_2 (MPa)	Poisson's Ratio	Shear Modulus G_{12} (MPa)	Ultimate strength (MPa)
0.13	70000	7000	0.25	5000	800

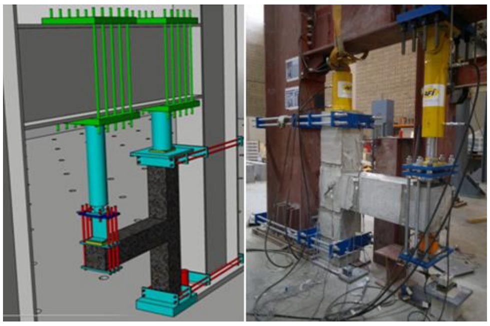

Fig. 2 Schematics of testing arrangement

values were obtained from the product data sheet provided by the manufacturer.

2.3 Test setup

The test setup for applying monotonic and cyclic loading at the end of the beam is shown schematically in Fig. 2. The BCJs were tested in a steel loading frame. The BCJ specimen was held in place using a clamping system attached at the bottom and top of the column. A clamping system at the tip of the beam was used for the application of push/pull loads using a hydraulic jack. A second hydraulic jack was placed on the top of the column to apply the desired axial load on the column. Several sensors were attached to the test specimen to measure the load, displacement and strains. A load cell was placed on the top of the column and the tip of the beam to measure the axial load. A wire type linear voltage displacement transducer (LVDT) was applied to measure the tip displacement of the beam. LVDT's were attached at the joint of the test specimen to measure the crack widths at a typical diagonal crack. Two LVDT's were attached at the top and bottom of the column to measure the transverse movements during displacement application at the tip of the beam. Strain gauges were attached on the top of the concrete surface in the joint region and the beams and on the surface of the CFRP sheets to monitor the strains. Concrete surface strain gauges were also attached on both the compression and tension sides of beam and column to measure the strains on the surface of the concrete. In order to measure the strain in the steel bars, special strain gauges were attached to the bars and protected from the concrete and moisture. Fig. 3 schematically shows the location of the strain gauges on each test specimen.

All BCJs were tested under displacement control. A constant axial load of 150 kN was applied on the top of the column for each specimen. Thereafter, a displacement was applied to the tip of the beam on both the push and pulls sides, and increased until the failure of the specimens in cyclic load tests.

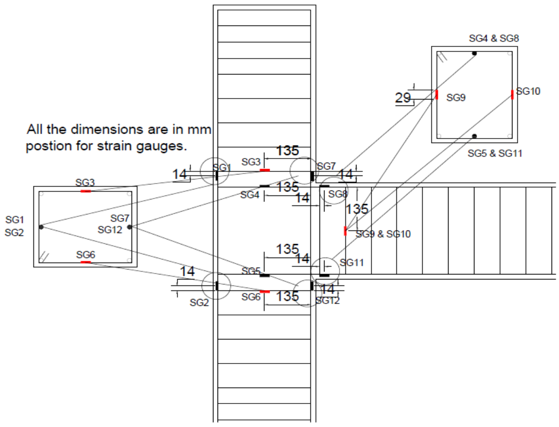

Fig. 3 Locations for strain gauges for reinforcement steel bar

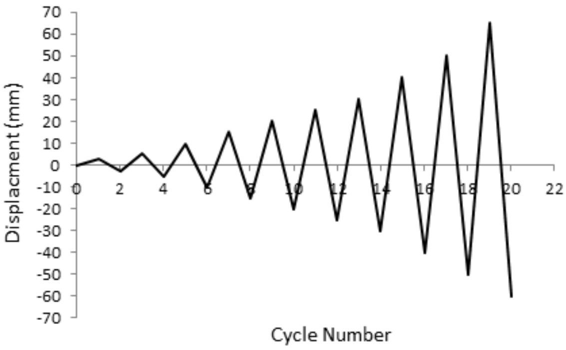

Fig. 4 Cyclic load applied at the tip of the beam

2.4 Load patterns

The BCJs joints were tested under monotonic and cyclic loading up to failure. The loading displacement-control at the end of the beam was applied incrementally. The applied displacements under cyclic loading consisted of an initial 0.04% drift followed by intervals at 0.288%, 0.6%, 1.11%, 1.66%, 2.22%, 2.77%, 3.33%, 4.44%, and 7.22% drift. Each drift step consisted of one cycle of push and pull. The cyclic load pattern and drift ratios are shown in Fig. 4.

2.5 Configuration of retrofitted BCJ with CFRP sheet

The BCJs were retrofitted using CFRP sheets. One layer of the CFRP sheet was wrapped diagonally on the beam-column joint. A 20cm wide CFRP sheet was attached to the surface using Sika-Dur 300 epoxy. The details of retrofitted specimen are shown in Fig. 5. The CFRP sheet with epoxy resin was then allowed to cure for a period of 7 days, as shown in Fig. 6(a) and Fig. 6(b), prior to testing under cyclic loading.

3. Finite Element Modeling (FEM)

A 3-D nonlinear finite element simulation of the BCJ was carried out using the commercial finite element software ABAQUS. The information here is presented to demonstrate the use of concrete damage plasticity model with an appropriate material models and interaction between different elements to correctly capture the actual performance of BCJ. The finite element model of the BCJ included nonlinear behavior due to the cracking and crushing of concrete and yielding of the steel bars. The concrete plastic damage model (CDP) developed by Lubliner *et al.* (1989) and extended by Lee and Fenves, (1998) was utilized to model the concrete. This CDP is the most commonly used model for simulating the performance of concrete by many researchers such as (Al-Osta *et al.* 2018, Kalyana Rama *et al.* 2017, Roth *et al.* 2010, Thirumalaiselvi *et al.* 2016). The steel rebar was modelled as elastic-plastic material. The CFRP was modelled as linear elastic lamina.

3.1 Material models

The CDP in ABAQUS for the concrete needs the uniaxial stress-plastic strain data and damage parameters of concrete in tension and compression as shown in Figs. 7 and 8. The material parameters used in CDP for concrete are shown in Table 5. The concrete damage parameters in compression and tension were computed based on the equations given by Birtel and Mark (2006)

$$d_c = 1 - \frac{\sigma_c E_c^{-1}}{\varepsilon_c^{pl}(\frac{1}{b_c} - 1) + \sigma_c E_c^{-1}} \tag{1}$$

Step 1: Applying epoxy to concrete surface | Step 2: A attachment of first diagonal strip | Step 3: A attachment of second diagonal strip | Step 4: A attachment of strips to other face of the joint | Step 5: Applying epoxy to concrete surface | Step 6: A attachment of strips to face of column and beam

Fig. 5 Retrofitting process of BCJ

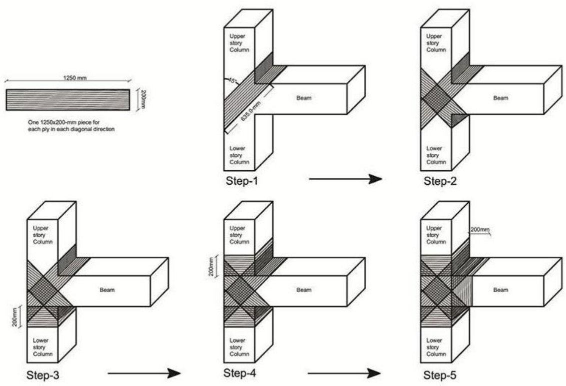

(a) CFRP application schemes

(b) Specimen with CFRP

Fig. 6 Retrofitting with CFRP (a) scheme model for applying the CFRP sheet (b) and specimen after applying CFRP

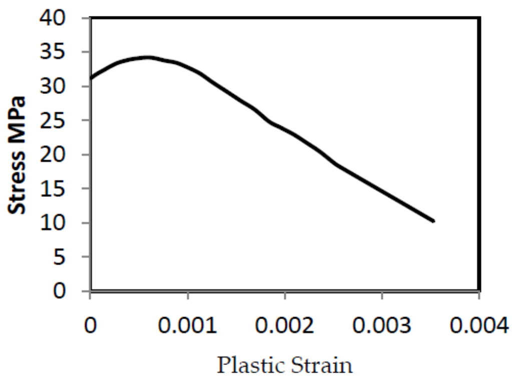

(a) Compression

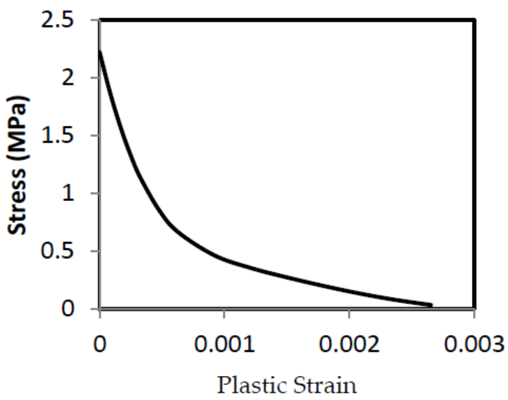

(b) Tension

Fig. 7 Stress-plastic strain curve for concrete under (a) Compression and (b) Tension

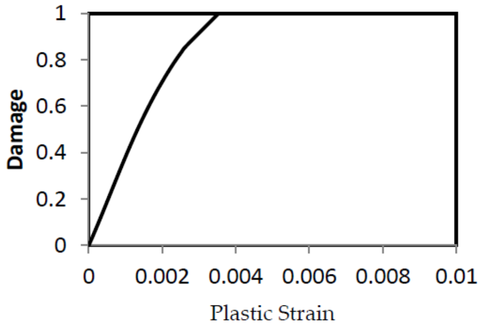

(a) Compression

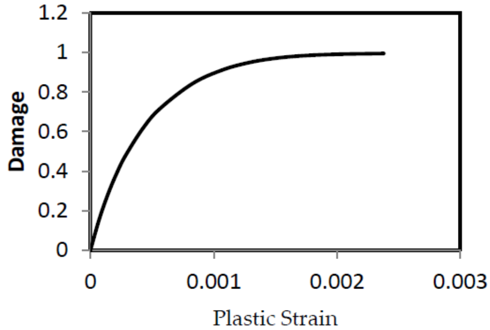

(b) Tension

Fig. 8 Stress-damage of concrete under (a) Compression and (b) Tension

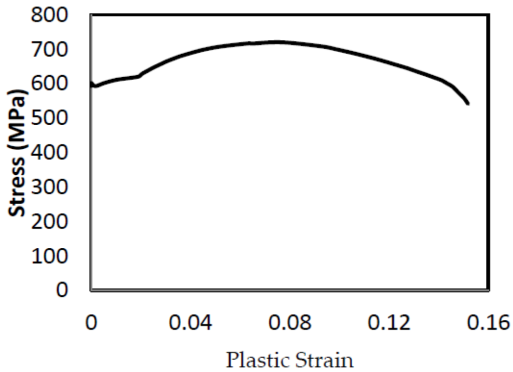

Fig. 9 Stress-damage of concrete under (a) Compression and (b) Tension

$$d_t = 1 - \frac{\sigma_t E_c^{-1}}{\varepsilon_t^{pl}(\frac{1}{b_t} - 1) + \sigma_t E_c^{-1}} \qquad (2)$$

where: d_c and d_t concrete damage parameters in compression and tension, respectively; σ_c and σ_t = compressive and tensile stresses; E_c concrete elastic modulus; ϵ_c^{pl} and ϵ_t^{pl} = plastic strain corresponding to compressive and tensile stress, respectively; b_c and b_t = constants for concrete damage parameters in compression and tension, respectively, with range $0 < b_c$ and $b_t < 1$.

For reinforcing steel, the stress-plastic strain curve obtained from the uniaxial test conducted on reinforcing steel is shown in Fig. 9. The CFRP material properties adopted in this study are shown in Table 4. The subscripts in Table 4 represent the principal material directions of the CFRP lamina.

Table 5 Value of parameters used in concrete damage plasticity model

Mass Density (Tons/mm^3)	Young's Modulus (MPa)	Poisson's Ratio	Dilatation Angle Ψ (Degree)	Eccentricity ε	f_{bo}/f_{co}	b_c/b_t
2.4E-009	26000	0.18	36	0.1	1.16	0.67

Table 6 Element types used in the model

Part	Element	Element description
Concrete	C3D8R	A 8-noded linear brick, reduced integration
Steel	T3D2	A 2-noded Linear 3D truss
CFRP	S4R	A 4-noded doubly curved thin or thick shell, reduced integration,

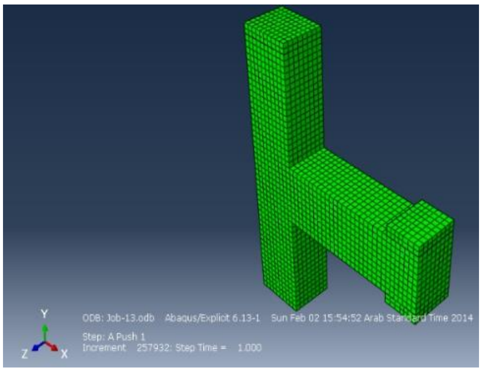

Fig. 10 3D FE model and mesh of BCJ

3.2 Finite element mesh and boundary conditions

The Finite element simulation of the BCJs tested in the experimental program was carried out using the commercial software ABAQUS using dynamic explicit analysis. The concrete cross section in the BCJ was modelled using the 8-nonded linear brick element (C3D8R) and the reinforcing steel embedded in concrete using the element T3D2, which is a 2-noded linear 3D truss as shown in Table 6. A 4-noded doubly curved thin or thick shell element (S4R) was used for the CFRP sheets, which was assumed to be perfectly bonded to the concrete. The 3D finite element model of the BCJ and the concrete FE mesh is shown in Fig. 10. The displacement is applied at the tip of the beam, which is constrained in the *y*-direction as shown in Fig. 11. The elements on the top surface of the column are restrained against translation in the *x*-and *z*-direction, whereas the bottom surface of the column is restrained against translation in the *x*, *y*, and *z*-direction. An axial load of 150 kN is applied by a hydraulic jack at the top of the column and is kept constant during the load application.

4. Results and discussion

4.1 Analytical computation of load capacity

The theoretical ultimate loads of RC BCJ specimens was computed in flexural (P_{uf}) based on conventional mechanics McCormac and Brown (2015) and the joint shear

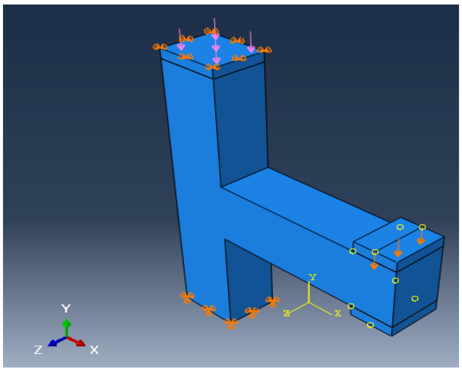

Fig. 11 Applied loads and boundary condition

(P_{us}) by using an empirical equation (ACI 352R-02). The joint shear strength as given in Eq. (3) depends on the parameter γ, which differs based on the joint type and classification. The value of γ for the specimens tested in the experimental program can vary due to the variation in the degree of confinement. The maximum shear capacity of joints as per the ACI 318-05 code is given by

$$V_{jr} = 0.083\gamma\sqrt{f_c'}\,b_j h_c \tag{3}$$

where V_{jr} is the maximum shear strength of the joint, the value of γ depends on the connections detailing and the magnitude of the seismic, b_j is the effective width of the joint, and h_c is the column dimension in the joint shear direction. The ACI code equation for the shear strength of joints does not take into consideration the effect of axial load on the column.

The shear capacity of the BCJs can be computed using the measured strains in the beam flexural steel during the load tests at the ultimate load P_u. The joint shear capacity (V_{je}) at the ultimate load condition of the non-retrofitted BCJ specimens can be calculated using the following equilibrium equation

$$V_{je} = T_s - V_{nc} \tag{4}$$

$$T_s = \varepsilon_s \times E_s \times A_s \tag{5}$$

$$V_{nc} = M_{nc}/Column\ shear\ span \tag{6}$$

where T_s is the total tensile force transferred from the flexural steel to the joint and V_{nc} is the shear force transferred by the column to the joint, ε_s is the actual tensile strain developed in the flexural steel bars at the ultimate load and A_s is the area of the flexural steel in the beams.

CFRP strengthening of the BCJs results in enhancement of the shear capacity of the shear deficient joints. A truss analogy proposed by PRIESTLEY (1997) can be used for predicting the shear capacity of the CFRP retrofitted BCJs. The shear capacity of the joint is computed by adding the CFRP sheet contribution. The tensile force F_{cfrp} developed in the CFRP sheet can be calculated from the effective strain ε_{fe} in the CFRP sheets (Eq. (7)). The effective strain is given as the lesser of 0.004 or 0.5 ε_{frpult} (ACI Committee-440 2008, Can/Csa 2012). E_f and A_f=modulus of elasticity and effective cross-sectional area of the CFRP sheets in the diagonal direction and ε_{frpult} is the ultimate strain of the

Table 7 Comparison of ultimate strength of specimens

Specimens (Monotonic Loading)	fc' MPa	Exp. Ultimate Load P_u [kN]	Exp. Shear Strength (MPa)	ACI Shear Strength (MPa)	New γ	Theoretical Ultimate Load [kN] Shear Capacity P_{us}	Flexural Capacity P_{uf}	P_u/ P_{us}	P_u/ P_{uf}	Mode of Failure
BCJ-18MM-Bent In	31	98	4.62	4.36	13.5	92.4	137.6	1.06	0.71	Joint shear failure
BCJ-12MM-Bent Up	31	71	3.37	4.36	9.9	91.7	66.3	0.77	1.07	Flexural failure
BCJ-12MM-Bent In	31	72	3.26	4.36	9.9	96.1	66.3	0.75	1.09	Flexural failure
BCJ-18MM-Bent In CFRP	31	118	8.15	10.42	23.9	150.9	144.9	0.78	0.81	Flexural or Shear failure
BCJ-12MM-Bent Up CFRP	31	85	10.25	10.42	30.1	86.4	74.9	0.98	1.13	Joint shear failure
BCJ-12MM-Bent In CFRP	31	82	10.78	10.42	31.6	79.3	74.9	1.03	1.09	Joint shear failure

Table 8 Cracking, ultimate loads and displacements for control specimen under monotonic test

Specimen ID	First Diagonal Crack		Extended Diagonal Crack		Crack at Ultimate		Failure Mode
	Load (kN)	Displ. (mm)	Load (kN)	Displ. (mm)	Load (kN)	Displ. (mm)	
BCJ-Bent-Up-12MM	57	11.7	60	49	71.2	18.2	Flexural Failure
BCJ-Bent In-12MM	53	8.53	68	14.3	74	26.8	Flexural Failure
BCJ-Bent In-18MM	50	5.5	90	14.9	97	17.5	Joint Failure

Table 9 Cracking, ultimate loads and displacements for CFRP retrofitted specimen under monotonic test

Specimen ID	First Diagonal Crack		Extended Diagonal Crack		Crack at Ultimate		Failure Mode
	Load (kN)	Displ. (mm)	Load (kN)	Displ. (mm)	Load (kN)	Displ. (mm)	
BCJ-Bent-Up-12MM	80	21.7	79	30.3	84	27.6	Flexural Failure
BCJ-Bent In-12MM	66	10.7	66	29.7	85.3	14.7	Flexural Failure
BCJ-Bent In-18MM	112	21.2	94	34.4	118	19.8	Joint Failure

CFRP sheets provided by the manufacturer. The CFRP sheets' contribution to the horizontal or vertical direction of the shear capacity is calculated by Equation 8 and Equation 9, which give the total shear capacity of the CFRP retrofitted joint. The results for the analytical calculation are shown in Table 7.

$$F_{cfrp} = \varepsilon_{fe} \times E_f \times A_f \tag{7}$$

$$V_{cfrp} = F_{scfrp} \times Sin\ \theta \tag{8}$$

$$V_t = V_{cfrp} + V_j \tag{9}$$

4.2 Experimental results for BCJs under monotonic loading

Three types of BCJ specimens, each with and without retrofitting by CFRP, were tested under monotonic loading up to failure. Two BCJ specimens with 12 mm dia flexural steel, one bent-up into the columns and the other bent-in, and one BCJ with 18 mm dia flexural steel, were tested. The load versus the displacement curves for the non-retrofitted and CFRP retrofitted BCJs of the three types, under monotonic loading, are shown in Fig. 12. Table 8 shows the loads and the corresponding displacements at some critical stages during the loading history for the non-retrofitted specimens and Table 9 shows similar values for the CFRP retrofitted specimens.

4.2.1 Cracking of non-retrofitted BCJs under monotonic loading

The cracking response of the non-retrofitted and the CFRP retrofitted specimens are shown in Figs. 13 and 14 respectively for the three types of BCJ specimens loaded to failure under monotonic loading.

In all non-retrofitted BCJ specimens, first a flexural crack was developed at the interface of the beam and the column. For the 12 mm dia flexural steel BCJ specimens the crack developed at 24 kN and 26 kN, whereas it was about 50% for the BCJ specimen with 18 mm dia flexural steel. This was followed by several flexural cracks in beams away from the joint as shown in Fig. 13. These cracks occurred at some distance away from the BCJ interface at a load of about 38 kN in the two 12 mm dia BCJ specimens.

In the 18 mm dia BCJ specimen. Very fine cracks were formed. The first diagonal crack in the joint region was initiated in the three beams at an approximately similar level of applied load, with the BCJ specimen with12 mm dia bars bent up in column being 10% higher (57 kN) compared to the BCJ specimen with 18 mm dia bars. The diagonal crack in the 18 mm dia BCJ occurred at 5.5 mm displacement as compared to 11.7 mm for the 12 mm dia BCJ with bent up bars.

4.2.2 Failure mode and load capacity of non-retrofitted BCJs under monotonic loading

Both 12 mm dia BCJ specimens failed in flexure with the development of a wide flexural crack at the interface and spalling of the concrete from the sides of the joint as seen in Figs. 13(a) and 12(b). It is evident that the flexural failure at the BCJ interface leads to the penetration of the cracking/yielding zone into the joint. The penetration of the failure zone into the joint is not desirable for a BCJ, which

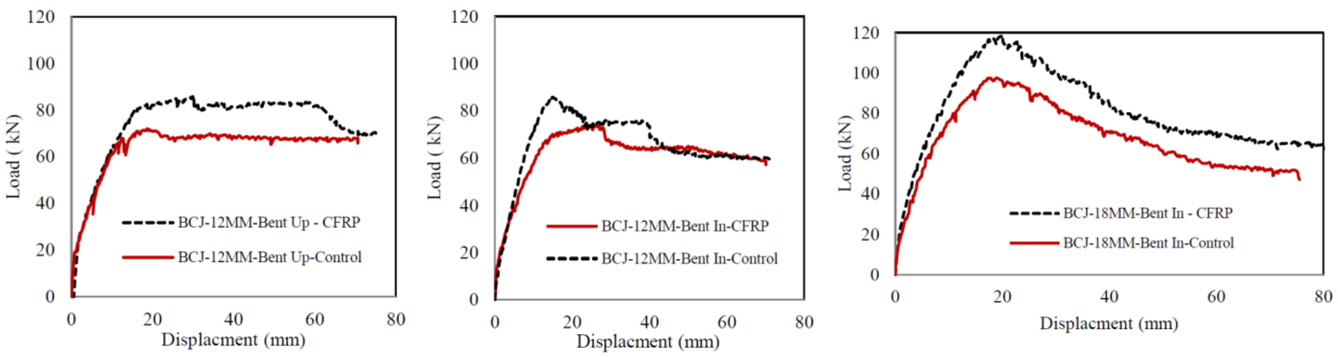

(a) Specimen BCJ- Bent Up - 12MM (b) Specimen BCJ- Bent In - 12MM (c) Specimen BCJ- Bent In - 18MM

Fig. 12 Load-displacement curves for non-retrofitted and CFRP retrofitted BCJs under monotonic loading

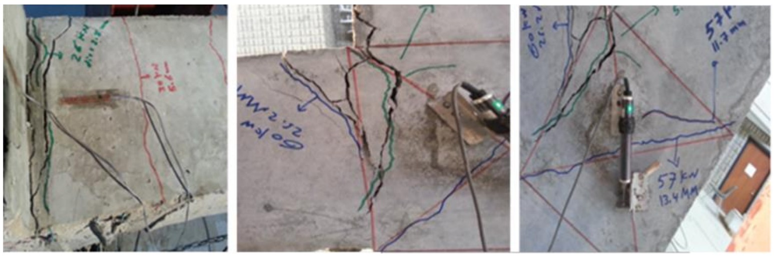

(a) BCJ-Bent-Up-12 mm specimen

(b) BCJ-Bent-In-12 mm specimen

(c) BCJ-Bent-In-18 mm specimen

Fig. 13 Crack development non retrofitted BCJs under monotonic loading

is designed to fail in flexure. The flexural crack should occur at some distance away from the interface. In the 18 mm dia BCJ specimen a wide diagonal crack developed in the joint at failure, showing a typical joint shear failure (Fig. 13(c)).

The ultimate load capacity of both 12 mm dia BCJ specimens are of the same order (71.2 kN and 74 kN), whereas the 18 mm dia BCJ specimen has an enhanced load capacity of 97 kN, being about 35% higher than the other two specimens. The flexurally over reinforced specimen (18 mm dia BCJ) leads to a joint failure, which is undesirable, even though the ultimate load capacity is higher.

4.2.3 Failure mode and load capacity of CFRP retrofitted BCJs under monotonic loading

Contrary to the flexural failure at the BCJ, interface in the non-retrofitted BCJ specimens with 12mm dia bars, flexural failure in the CFRP retrofitted BCJs occurred away from the beam-column interface. The CFRP retrofit resulted in local failure away from the BCJ interface and this prevented the undesirable shear failure in the joints. The shear strength of the 12 mm dia BCJ specimens is close to the flexural strength of the beam (Table 7). CFRP strengthening results in a significant enhancement of the load at which the first diagonal crack occurs in the joint. In the 12 mm dia bent up bar BCJ, the diagonal cracking resistance is increased by 40% compared to the 25% increment in the BCJ 12 mm dia bent-in specimen. In the 18 mm dia BCJ specimen, an approximate 125% increase in the load capacity occurs at the first diagonal crack due to

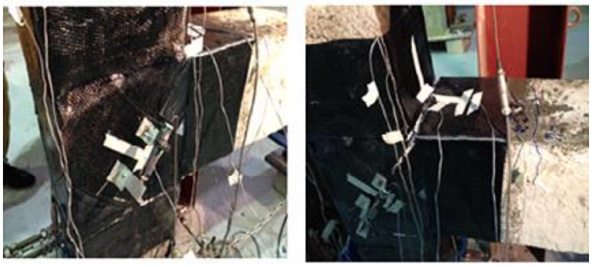

(a) BCJ-Bent-Up-12 mm specimen

(b) BCJ-Bent-In-12 mm specimen

(c) BCJ-Bent-In-18 mm specimen

Fig. 14 Crack development CFRP retrofitted BCJs under monotonic loading

CFRP strengthening. Once the diagonal crack develops, and in the joint and the CFRP ruptures, the ultimate load capacity does not increase significantly.

In the CFRP retrofitted BCJ specimen with 12 mm dia bent up bars, the ultimate load capacity is 84.1 kN at 27.6 mm displacement. A flexural crack first developed at some distance from the BCJ interface at load 48 kN and displacement 6.4 mm (Fig. 14(a)). The second flexural crack at the BCJ interface occurs at a load 74 kN at 14.2 mm displacement. The CFRP sheet ruptures in the weak direction at the joint at a load of 80 kN (displacement 21.7 mm). The rupture of the CFRP sheet in the strong direction occurs at load 79 kN and displacement 30.3mm as shown in Fig. 14(a). The maximum strain at the time of the rupture of the CFRP was 0.003894μs. The retrofitted sample enhances the load displacement response of the BCJ for 19.7%.

Fig. 14(b) shows the failure of the CFRP strengthened BCJ with 12 mm dia flexural steel bent in the joint. The ultimate load capacity of this BCJ specimen was similar to the 12 mm dia bent up bar specimen (85.3 kN and 14.7 mm displacement). The displacement at failure is significantly lower as compared to the bent up bar specimen. The first visible crack was a flexural crack occurring at some distance away from the BCJ interface at a load of 24 kN with the second flexural crack occurring at the BCJ interface at a load 42 kN. The first rupture of the CFRP sheet in the weak direction occurred at load 66 kN and displacement 10.7 mm. After that, the rupture of the CFRP sheet in the strong direction occurred at the same load (66 kN) and increased displacement of 29.7 mm, as shown in Fig. 14(b). The CFRP strengthening increased the load carrying capacity by 12.8%.

The ultimate load capacity of the BCJ with 18 mm dia bars was 118.3 kN with a corresponding displacement of 19.8 mm. The first flexural crack developed at some distance from the BCJ interface at a load of 62 kN (displacement 5.2 mm). Several flexural cracks occurred in the beam at a load of 94 kN and a displacement of 11 mm. The CFRP sheet failed in the weak direction at a load of 112 kN and displacement 21.2 mm. Failure of the CFRP sheet in the strong direction started at a reduced load of 94 kN. Complete rupture of the CFRP sheet occurred during the softening phase at a load of 76 kN and a displacement of 43.9 mm (Fig. 14(c)). The maximum strain at the time of the rupture of the CFRP was 0.005336 μs. CFRP strengthening of this specimen results in an enhancement of the ultimate capacity by 20.8%.

4.3 Experimental results for BCJs under cyclic loading

Three types of BCJ specimens, each with and without retrofitting by CFRP, were tested under monotonic loading up to failure. Two BCJ specimens with 12 mm dia flexural steel, one bent-up into the columns and the other bent-in, and one BCJ with 18 mm dia flexural steel, were tested. The load versus the displacement curves for the non-retrofitted and CFRP retrofitted BCJs of the three types, under monotonic loading, are shown in Fig. 12. Table 8 shows the loads and the corresponding displacements at some critical stages during the loading history for the non-

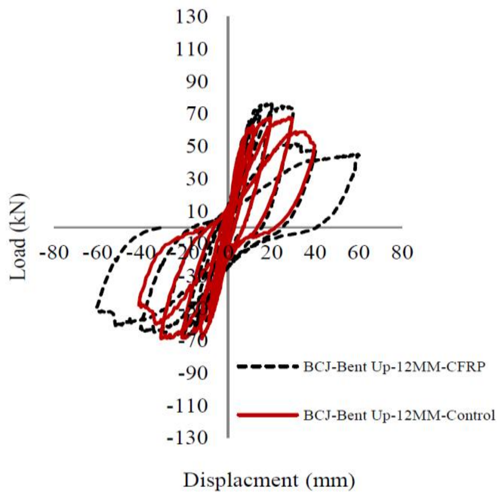

(a) Specimen BCJ- Bent Up - 12MM

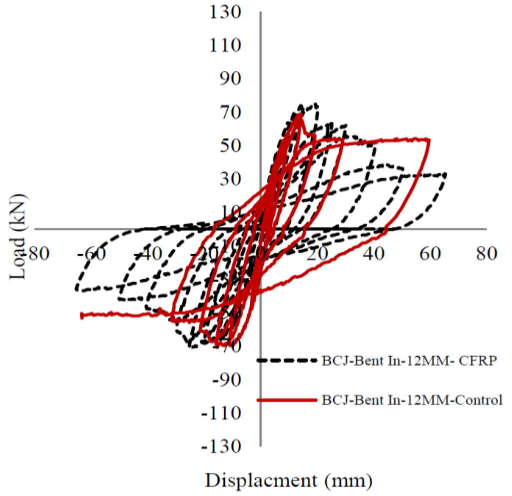

(b) Specimen BCJ- Bent In - 12MM

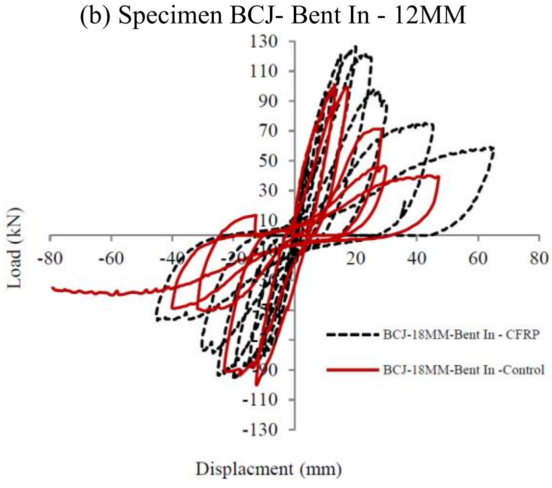

(c) Specimen BCJ- Bent In - 18MM

Fig. 15 Load-displacement curves for non-retrofitted and CFRP retrofitted BCJs under cyclic loading

(a) BCJ-Bent-Up-12mm Specimen

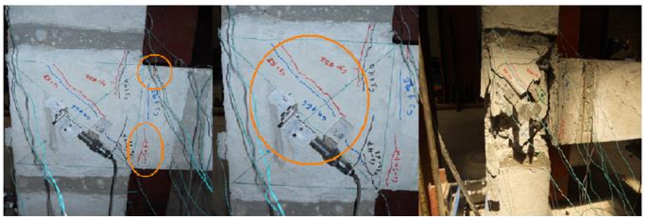

(b) BCJ-Bent-In-12mm Specimen

(c) Specimen BCJ- Bent In - 18MM

Fig. 16 Crack development CFRP retrofitted BCJs under monotonic loading

retrofitted specimens and Table 9 shows similar values for the CFRP retrofitted specimens.

4.3.1 Crack development and cyclic load-displacement response of non-retrofitted BCJs

The cyclic load-displacement response for the non-retrofitted and CFRP retrofitted BCJ specimens up to failure are shown in Fig. 15 for the three types of BCJ specimens tested under the experimental program. Tables 10 and 11 show the values of the loads and displacements at various critical stages during the push and pull cycles and the mode of failure.

In both BCJ-12MM BCJs, with bent-up and bent-in bars, the first crack formed in the specimen was at the beam-column interface during the first cycle both at the top, the bottom during the push, and the pull displacement. The cracking load was 25 kN (push) and 2.2 mm, and 20 kN (pull). In the BCJ-18MM BCJ specimen, this crack occurred at 45 kN, an enhancement of 80%, which can be attributed to the higher reinforcement ratio. Under increasing load minor flexural cracks developed in the beam away from the interface, and a diagonal crack also developed in the joint region. The diagonal crack developed at a 53 kN load in both BCJ-12MM specimens and 60 kN in the BCJ-18MM BCJ. The diagonal cracks initiating at the joint progresses towards the center. Diagonal cracks were formed in both directions as shown in Figs. 16(a), (b) and (c).

4.3.2 Ultimate load and mode of failure of non-retrofitted BCJs

The ultimate load for the BCJ-12MM Bent-up occurred at 67.2 kN (Push) and 68.8 kN (Pull), whereas, the Bent-in BCJ specimen failed at loads similar in magnitude i.e., 67.8 kN (Push) and 69.4 kN (Pull). The 12 mm dia BCJ specimen with bent-in bars, however, showed higher

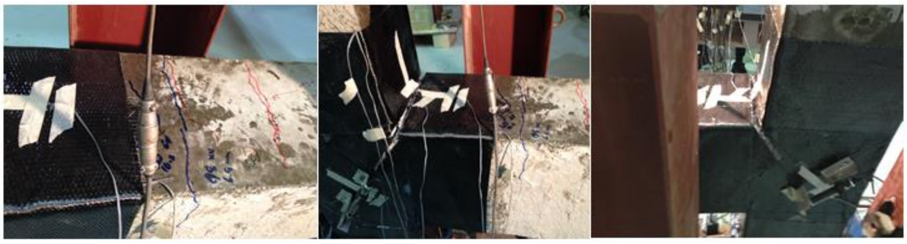

(a) BCJ-Bent-Up-12 mm specimen

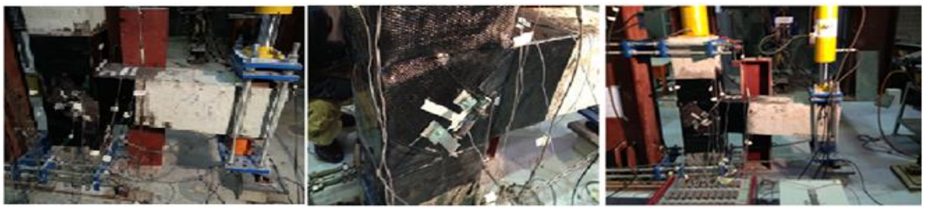

(b) BCJ-Bent-In-12 mm specimen

(c) Specimen BCJ- Bent In - 18MM

Fig. 17 Crack development CFRP retrofitted BCJs under monotonic loading

Table 10 Cracking, ultimate loads and displacements for control specimen under cyclic test

Specimen ID	First Diagonal Crack		Extended Diagonal Crack		Crack at Ultimate		Failure Mode
	Load (kN)	Displ. (mm)	Load (kN)	Displ. (mm)	Load (kN) Push/Pull	Displ.(mm) Push/Pull	
BCJ-Bent-Up-12MM	53 (Push)	6.49 (Push 3rd)	66 (Push 4th)	-	67.2/68.8	18.9/12.1	Flexural Failure
BCJ-Bent In-12MM	53 (Push 3rd)	-	66 (Push 4th)	40 (Push)	67.8/69.4	-	Flexural Failure
BCJ-Bent In-18MM	60 (Push)	5.59 (Push)	-	-	99/100.3	-	Joint Failure

Table 11 Cracking, ultimate loads and displacements for CFRP retrofitted specimen under cyclic test

Specimen ID	CFRP Rupture in weak direction		CFRP Rupture in Strong direction		Crack at Ultimate		Failure Mode
	Load (kN)	Displ. (mm)	Load (kN)	Displ. (mm)	Load (kN) Push/Pull	Displ. (mm) Push/Pull	
BCJ-Bent-Up-12MM	72 (Push)	6.49 (Push)	46 (Push)	40 (Push)	76.1/67.7	19.95/18.8	Flexural Failure
BCJ-Bent In-12MM	72 (Push)	-	70 (Push)	30.3 (Push)	73.2/70.3	-	Flexural Failure
BCJ-Bent In-18MM	124 (Push)	5.59 (Push)	85 (Push)	-	124.7/92.9	-	Joint Failure

ductility as compared to the bent-up bar specimen, with a higher energy dissipation. The 12 mm dia BCJs showed diagonal cracks in both directions in the joint region at failure, together with a wide crack at the BCJ interface for both Bent-up and Bent-in bars as shown in Fig. 16(a) and 16(b). A clear *X*-shaped cracks at failure was observed for the Bent-up bars, whereas for Bent-in bars spalling of the cover took place following the *X*-shaped cracks as shown in Fig. 16(b). The diagonal cracks at failure penetrated into the column at the backside. The ultimate load capacity of the 18-MM BCJ specimen was 99 kN/100 kN in the Push/Pull direction. Failure occurred in the joint with failure mode characterized by *X*-shaped diagonal cracks formed in the joint as shown in Fig. 16(c). At the backside of the joint, the concrete cover spalled off at failure exposing the reinforcing bars.

4.3.3 Failure mode and load capacity of CFRP retrofitted BCJs under cyclic loading

CFRP strengthening of the 12-MM dia bent-in and bent-

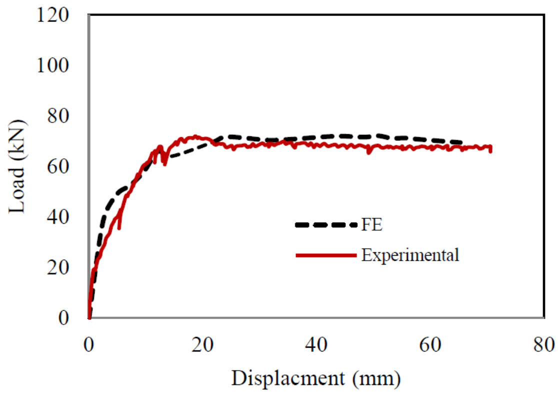

(a) BCJ- Bent Up - 12MM specimen

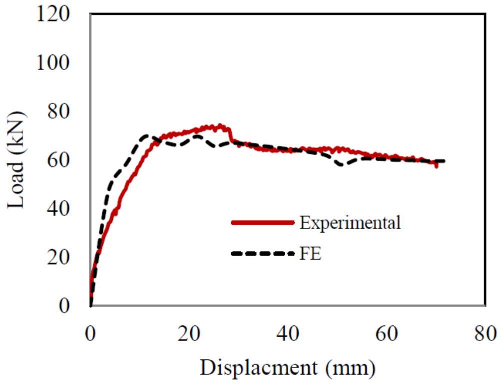

(b) BCJ- Bent In - 12MM specimen

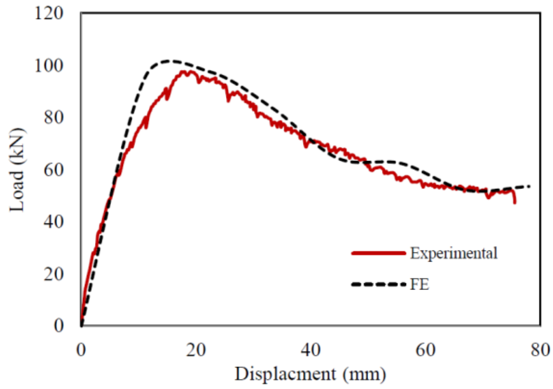

(c) BCJ- Bent In - 18MM specimen

Fig. 18 Experimental and FE Load displacement response for non-retrofitted specimen

up BCJ resulted in an increase of about 10% in the ultimate load capacity. The mode of failure was a wide crack at the BCJ interface with a rupture in the CFRP sheets at the joint. However, the first flexural cracks were formed in these specimens beyond the 200 mm length of the CFRP sheets on the beams. The number of plies of the CFRP sheets needs to be added to ensure that the failure would remain in this region and not move to the BCJ interface. CFRP strengthening of the 18-MM BCJ specimen, however, resulted in a significant enhancement of about 27.5% in the ultimate load capacity. The ultimate load was 124.7 kN/92.2 kN in the Push/Pull direction and the CFRP rupture took place in the joint region. Enhanced ductility and energy dissipation is evident in Fig. 15(c). The lower capacity in the pull direction can be attributed to the damage in the CFRP bonding at the bottom BCJ interface during the push cycle. In the last two cycles, the beam-column interface of the specimen was badly damaged with a concrete cover spalling off from one side of the joint exposing the joint reinforcement. Fig. 17 shows the cracking and failure in the BCJ with three types of CFRP retrofitted specimens.

4.4 Results from numerical simulation of BCJs

Simulation of the BCJs subjected to monotonic loading up to failure was carried out in the ABAQUS environment using the concrete damage plasticity based constitutive model detailed in Section 3. The evolution of damage in concrete which reflects the development of cracks and joint deterioration was investigated. The experimental and finite element results of the load-displacement response of the 12MM-BCJ specimens with bent-in or bent-up rebars are shown in Fig. 18. The experimental response, including the ultimate load and the displacement up to failure, was captured in the FE simulation with a good degree of accuracy. After the initial elastic response and the development of the first crack at the interface, a stiffer response is observed in the FE simulation as evident in Fig. 18(a) and (b). Fig. 19 shows the damage in the beams and the joints of the two 12-MM BCJ specimens. Full depth flexural damage at the BCJ interface and flexural cracking away from the interface extending to a distance of about 250 mm can be observed in the two specimens. It can be seen that the yield zone of the flexural steel at the BCJ interface extends into the joint. The experimental and finite element response of the BCJ with 18-MM dia bars is shown in Fig. 18(c). It can be seen that the FE simulation captured the experimental response with a very good degree of accuracy. The initial response from the FE model, up to a load of about 65 kN, overlaps the experimental results. After the development of the initial crack, the finite element response shows a slightly deviated stiffer response up to the peak load. The descending load-displacement response is captured with a very good degree of accuracy. The CFRP sheet used to strengthen the BCJ was incorporated in the finite element model in ABAQUS. A cohesive contact model is used to model the CFRP applied on the concrete surface.

The experimental and FE load-displacement response of the CFRP retrofitted BCJ are shown in Fig. 20 for the three types of specimen. Both 12-MM BCJ Bent-In and Bent-Up specimens show a slightly stiffer response after the initial elastic response up to the point of cracking as shown in Fig. 20(a) and 20(b). Fig. 21 shows the damage and cracking in the BCJ from the FE simulation for the BCJ-12mm with CFRP. The damage is more pronounced away from the BCJ interface in the beam and more pronounced as compared to the non-retrofitted specimen. The stresses developed in the CFRP sheet in the joint region for the 12-MM BCJ specimens in the direction of the fiber at the yielding and the ultimate load are shown in Fig. 22.

The load-displacement response for the 18-MM bar BCJ specimen retrofitted with CFRP is shown in Fig. 20(c). From the start of the loading, the finite element model portrays a stiffer response up to the peak load, with a slightly higher load at a smaller displacement compared to

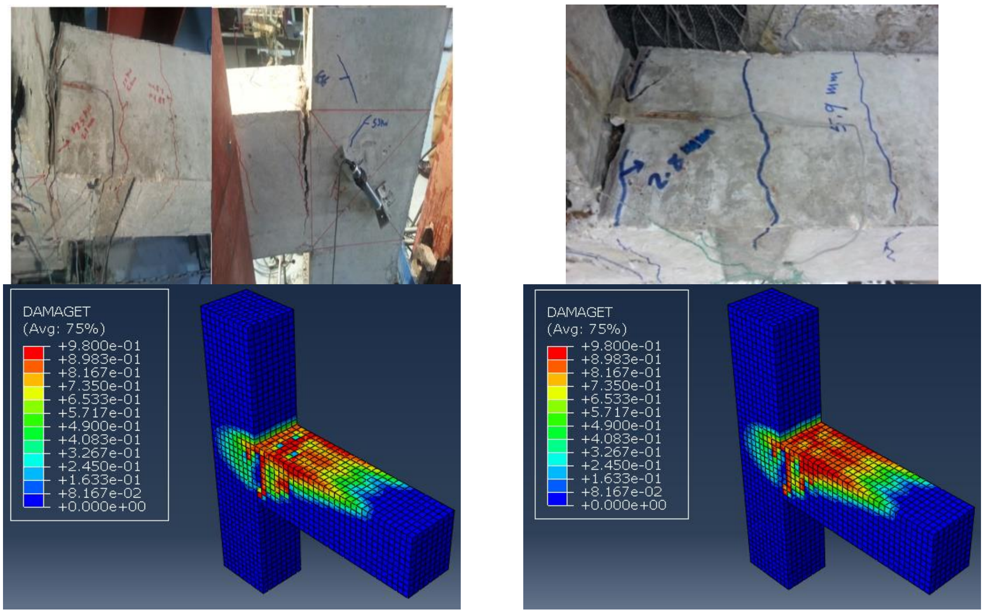

(a) BCJ-Bent-In-12mm Specimen (Δ=5.3 mm) (b) BCJ-Bent-Up-12mm Specimen (Δ=5.6 mm)

Fig. 19 Tension damage and cracking from FE simulation for BCJ-12MM without CFRP

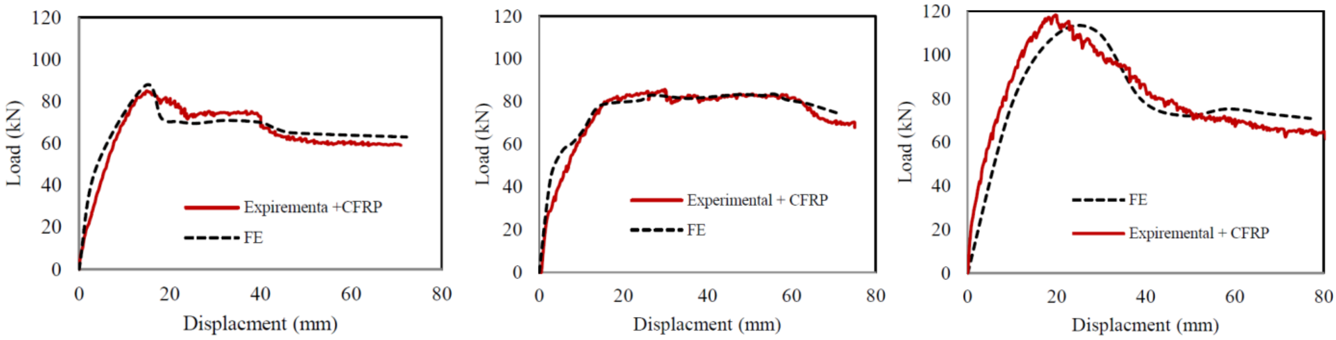

(a) BCJ-Bent-In-12mm Specimen (b) BCJ-Bent-Up-12mm Specimen (b) BCJ-Bent-Up-18mm Specimen

Fig. 20 Load displacement response for BCJ with CFRP

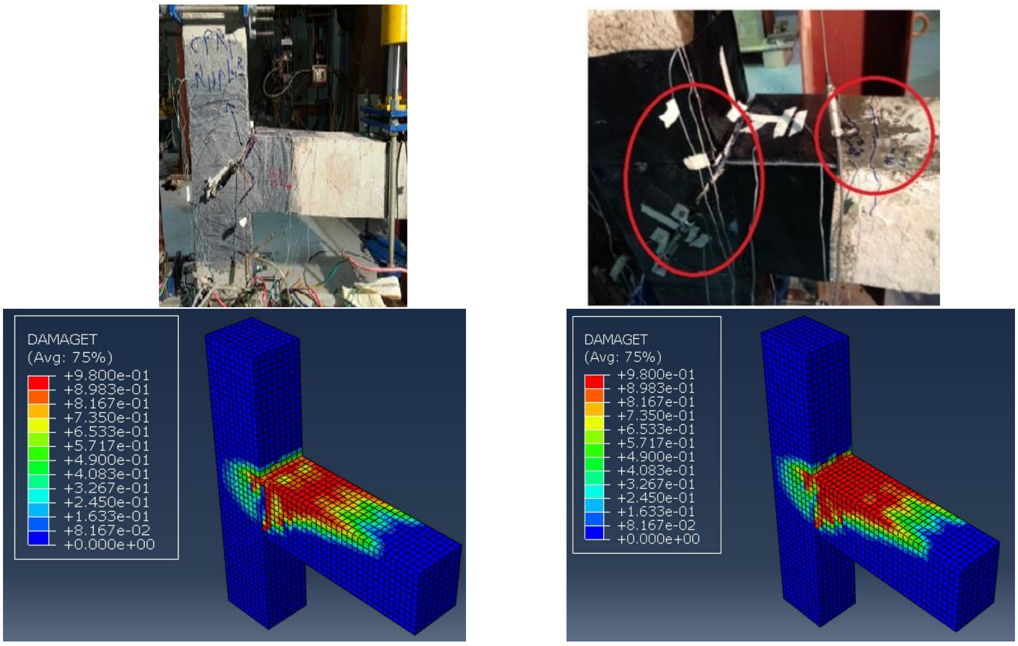

Tension damage-Bent In (At Δ=4.9 mm) Tension damage-Bent Up (At Δ=7 mm)

Fig. 21 Damage and cracking from FE simulation for BCJ-12mm with CFRP

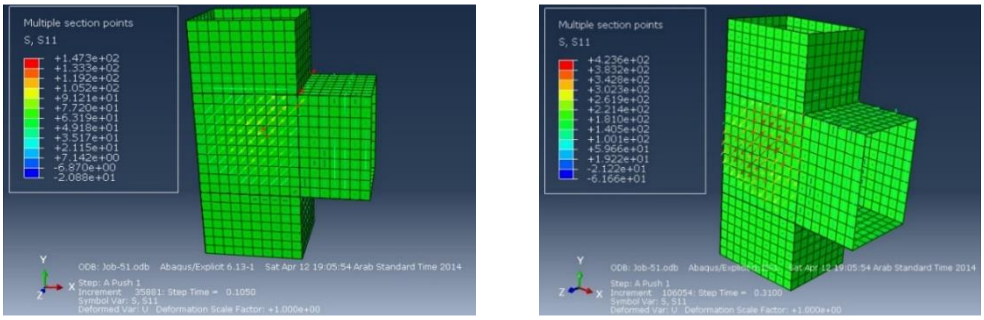

(a) At yielding load (Δ= 7 mm) -Bent In (b) At ultimate load (Δ=24.2 mm) -Bent In

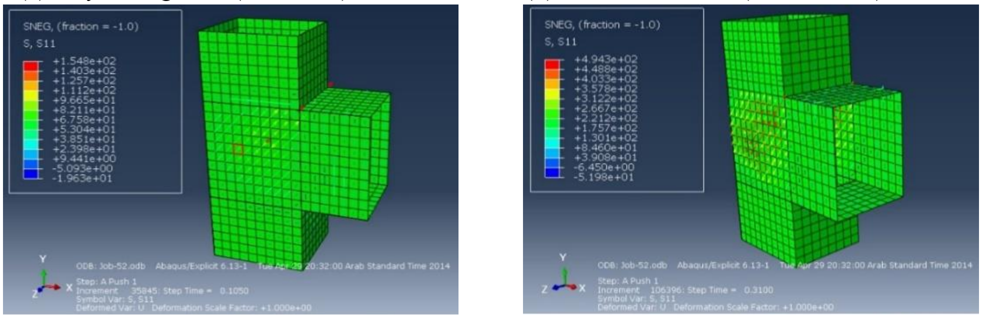

(c) At yielding load (Δ=7.35 mm)- Bent Up (d) At ultimate load (Δ=21.8 mm)- Bent Up

Fig. 22 Stress S11 in CFRP for BCJ-12MM specimens with CFRP

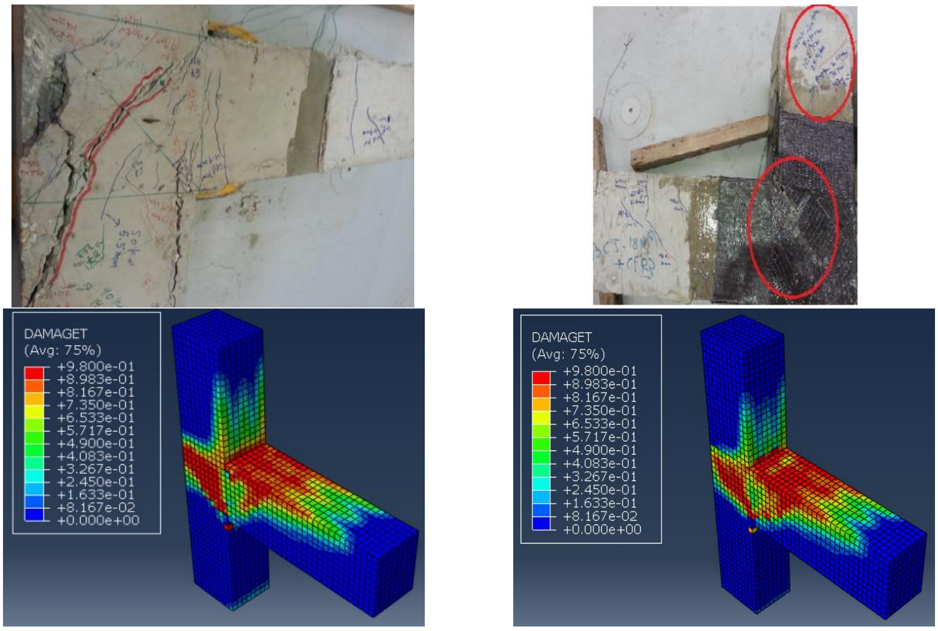

Specimen without CFRP (Δ=14 mm) Specimen with CFRP (Δ=10.5 mm)

Fig. 23 Tension damage and crack pattern for BCJ-18mm-Bent in without CFRP

the experimental data. Fig. 23 shows the tensile damage in the joint region with a diagonal crack which is captured in the FE simulation for both the retrofitted and non-retrofitted specimens.

5. Conclusions

Twelve non-retrofitted and CFRP-retrofitted exterior beam column joints were investigated under cyclic and monotonic loading until failure, followed by a non-linear FE simulation of these joints. The following conclusions can be derived from the investigations conducted.

1. The experimental results showed that the CFRP retrofitted BCJ with 12 mm dia flexural steel, bent up in the columns at the joints, gave a higher enhancement in the ultimate load capacity i.e., 19.6% as compared to the 12.9% in the 12 mm steel bent in the joint under monotonic loading. Under cyclic loading both flexurally deficient BCJs showed only 9% to 10% enhancement by CFRP retrofitting. The deterioration of the concrete at the top and bottom of the interface under reversed cyclic

loading and the yielding of both the top and bottom steel led to the lower enhancement. The failure mode in all of the 12 mm dia bar BCJs was due to the development of wide cracks at the beam-column joint interface with steel yielding and the yield zone penetrating into the joint and damaging the concrete in the joint close to the interface. CFRP strengthening showed a larger number of cracks in the beams away from the joint.

2. For BCJs with a higher reinforcement ratio (ρ=0.01%) with 18 mm dia flexural steel bent into the joint, both under monotonic and cyclic loading, the joint shear failure took place with a distinct *X*-shaped diagonal joint crack under cyclic loading. Both under monotonic and cyclic loading, the ultimate load capacities are higher as compared to the non-retrofitted specimen, being 20.8% and 27.5% higher respectively. Joint integrity remained intact for a large end displacement at the beam, in contrast to the non-retrofitted specimens with substantial damage to the joint region. Analytical computations showed that the joint shear capacity of the CFRP retrofitted specimen was of the same order as the flexural capacity. Failure took place with a rupture of the CFRP fabric in the joint region. This indicates that a larger number of the sheets would be needed in the joint region to change the failure mode from joint shear failure to flexural failure.

3. All of the BCJs were investigated experimentally. The FE simulation with the concrete damage plasticity constitutive model and the cohesive contact model between the CFRP and the concrete, captured the load-deformation response, ultimate load capacity, the softening curve after peak load and the failure mode with a good degree of replication. The FE simulation of the BCJs with 12 mm flexural reinforcements, showed distinct cracking at the interface and the joint region with a penetration of the yield zone into the joint. FE simulation of the 18 mm dia shear deficient BCJ, captured the *X*-shaped diagonal failure in the joint region. The damage mechanics approach in ABAQUS, coupled with the experimentally obtained parameters, captured the response of both non-retrofitted and retrofitted specimens with a high accuracy increasing the damage and cracking observed during the experiment.

4. The topmost conclusion of performed numerical analysis is that the use of concrete damage plasticity (CDP) constitutive model with an appropriate material models and interaction between different elements are important to appropriately capture the actual behavior of BCJ strengthens with CFRP sheets. Future study is needed to carry out a parametric study by using the developed FE model to further investigate the effect of thickness of CFRP sheets, reinforcement ratio and axial load levels of columns on the behavior of BCJs.

Acknowledgements

The authors would like to acknowledge the support provided by KFUPM through a research grant from the Office of the Deanship of Scientific Research, KFUPM, Dhahran 31261, Saudi Arabia, under Project No. RG1111-1/2. The support provided by the Department of Civil and Environmental Engineering and the Center for Engineering Research at Research Institute, KFUPM is duly acknowledged.

References

ACI 352R-02 (2002), Recommendations for Design of Beam-Column Connections in Monolithic Reinforced Concrete Structures, American Concrete Institute.

ACI Committee 440, ACI 440.2R-08 (2008), Guide for the Design and Construction of Externally Bonded FRP Systems, American Concrete Institute.

Ahmed, D., Baluch, M.H., Rahman, M.K. and Ilki, A. (2014), "Finite element modeling of seismic performance of low strength concrete exterior beam-column joints", *Seismic Evaluation and Rehabilitation of Structures*, Springer, Cham. https://doi.org/10.1007/978-3-319-00458-7_13.

Akguzel, U. and Pampanin, S. (2012), "Assessment and design procedure for the seismic retrofit of reinforced concrete beam-column joints using FRP composite materials", *J. Compos. Constr.*, **16**(1), 21-34. https://doi.org/10.1061/(ASCE)CC.1943-5614.0000242.

Al-Osta, M.A., Al-Khatib, A.M., Baluch, M.H., Azad, A.K. and Rahman, M.K. (2017), "Performance of hybrid beam-column joint cast with high strength concrete", *Earthq. Struct.*, **12**(6), 603-617. https://doi.org/10.12989/eas.2017.12.6.603.

Al-Osta, M.A., Al-Sakkaf, H.A., Sharif, A.M., Ahmad, S. and Baluch, M.H. (2018), "Finite element modeling of corroded RC beams using cohesive surface bonding approach", *Comput. Concrete*, **22**(2), 167-182. https://doi.org/10.12989/cac.2018.22.2.167.

Al-Osta, M.A., Khan, U., Baluch, M.H. and Rahman, M.K. (2018), "Effects of variation of axial load on seismic performance of shear deficient RC exterior BCJs", *Int. J. Concr. Struct. Mater.*, **12**(1), 46. https://doi.org/10.1186/s40069-018-0277-0.

Alhaddad, M.S., Siddiqui, N.A., Abadel, A.A., Alsayed, S.H. and Al-Salloum, Y.A. (2012), "Numerical investigations on the seismic behavior of FRP and TRM upgraded RC exterior beam-column joints", *J. Compos. Constr.*, **16**(3), 308-321. https://doi.org/10.1061/(ASCE)CC.1943-5614.0000265.

Alsayed, S.H., Al-Salloum, Y.A., Almusallam, T.H. and Siddiqui, N.A. (2010), "Seismic response of FRP-upgraded exterior RC beam-column joints", *J. Compos. Constr.*, **14**(2), 195-208. https://doi.org/10.1061/(ASCE)CC.1943-5614.0000067.

Antonopoulos, C.P. and Triantafillou, T.C. (2003), "Experimental investigation of FRP-strengthened RC beam-column joints", *J. Compos. Constr.*, **7**(1), 39-49. https://doi.org/10.1061/(ASCE)1090-0268(2003)7:1(39).

Bakir, P.G. (2003), "Seismic resistance and mechanical behaviour of exterior beam-column joints with crossed inclined bars", *Struct. Eng. Mech.*, **16**(4), 493-517. https://doi.org/10.12989/sem.2003.16.4.493.

Bedirhanoglu, I., Llki, A., Pujol, S. and Kumbasar, N. (2010), "Behavior of deficient joints with plain bars and low-strength concrete", *ACI Struct. J.*, **107**(3), 300. https://doi.org/10.1061/(ASCE)CC.1943-5614.0000156.

Bindhu, K.R., Jaya, K.P. and Manicka Selvam, V.K. (2008), "Seismic resistance of exterior beam-column joints with non-conventional confinement reinforcement detailing", *Struct. Eng. Mech.*, **30**(6), 733-761. https://doi.org/10.12989/sem.2008.30.6.733.

Birtel, V. and Mark, P. (2006), *Parameterised Finite Element Modelling of RC Beam Shear Failure*, Ababqus User's Conf.

Bruneau, M., Wilson, J.C. and Tremblay, R. (1996), "Performance of steel bridges during the 1995 Hyogo-ken Nanbu (Kobe, Japan) earthquake", *Can. J. Civil Eng*., **23**(3), 678-713. https://doi.org/10.1139/l96-883.

CAN/CSA-S806-12 (2012), Design and Construction of Building Structures with Fibre-reinforced Polymers, Canadian Standards Association, Ontario, Canada.

Carmo, R.N.F., Costa, H., Gomes, G. and Valença, J. (2017), "Experimental evaluation of lightweight aggregate concrete beam-column joints with different strengths and reinforcement ratios", *Struct. Concrete*, **18** (6), 950-961. https://doi.org/10.1002/suco.201600166.

Celik, O.C. and Ellingwood, B.R. (2008), "Modeling beam-column joints in fragility assessment of gravity load designed reinforced concrete frames", *J. Earthq. Eng.*, **12**(3), 357-381. https://doi.org/10.1080/13632460701457215.

Chalioris, C., Kosmidou, P.M. and Papadopoulos, N. (2018), "Investigation of a new strengthening technique for RC deep beams using carbon FRP ropes as transverse reinforcements", *Fiber.*, **6**(3), 52. https://doi.org/10.3390/fib6030052.

Chalioris, C.E. and Bantilas, K.E. (2017), "Shear strength of reinforced concrete beam-column joints with crossed inclined bars", *Eng. Struct.*, **140**, 241-255. https://doi.org/10.1016/j.engstruct.2017.02.072.

Chalioris, C.E., Favvata, M.J. and Karayannis, C.G. (2008), "Reinforced concrete beam-column joints with crossed inclined bars under cyclic deformations", *Earthq. Eng. Struct. Dyn*., **37**(6), 881-897. https://doi.org/10.1002/eqe.793.

De Vita, A., Napoli, A. and Realfonzo, R. (2017), "Full scale reinforced concrete beam-column joints strengthened with steel reinforced polymer systems", *Front. Mater*., **4**, 1-17. https://doi.org/10.3389/fmats.2017.00018.

Del Vecchio, C., Di Ludovico, M., Balsamo, A., Prota, A., Manfredi, G. and Dolce, M. (2014), "Experimental investigation of exterior RC beam-column joints retrofitted with FRP systems", *J. Compos. Constr*., **18**(4), 04014002. https://doi.org/10.1061/(ASCE)CC.1943-5614.0000459.

El-Amoury, T. and Ghobarah, A. (2002), "Seismic rehabilitation of beam-column joint using GFRP sheets", *Eng. Struct*., **24**(11), 1397-1407. https://doi.org/10.1016/S0141-0296(02)00081-0.

Ghobarah, A. and El-Amoury, T. (2005), "Seismic rehabilitation of deficient exterior concrete frame joints", *J. Compos. Constr*., **9**(5), 408-416. https://doi.org/10.1061/(ASCE)1090-0268(2005)9:5(408).

Ibrahim, A.M. and Sh Mahmood, M. (2009), "Finite element modeling of reinforced concrete beams strengthened with FRP laminates", *Eur. J. Sci. Res*., **30**(4), 526-541. https://doi.org/10.1016/j.conbuildmat.2011.07.018.

Kalyana Rama, J.S., Chauhan, D.R., Sivakumar, M.V.N., Vasan, A. and Murthy, A.R. (2017), "Fracture properties of concrete using damaged plasticity model-A parametric study", *Struct. Eng. Mech.*, **64**(1), 59-69. https://doi.org/10.12989/sem.2017.64.1.059.

Karayannis, C.G. and Chalioris, C.E. (2013), "Shear tests of reinforced concrete beams with continuous rectangular spiral reinforcement", *Constr. Build. Mater.*, **46**, 86-97. https://doi.org/10.1016/j.conbuildmat.2013.04.023.

Karayannis, C.G. and Sirkelis, G.M. (2008), "Strengthening and rehabilitation of RC beam-column joints using carbon-FRP jacketing and epoxy resin injection", *Earthq. Eng. Struct. Dyn*., **37**(5), 769-790. https://doi.org/10.1002/eqe.785.

Khan, M.I., Al-Osta, M.A., Ahmad, S. and Rahman, M.K. (2018), "Seismic behavior of beam-column joints strengthened with ultra-high performance fiber reinforced concrete", *Compos. Struct*., **200**, 103-119. https://doi.org/10.1016/j.compstruct.2018.05.080.

Le-Trung, K., Lee, K., Lee, J., Lee, D.H. and Woo, S. (2010), "Experimental study of RC beam-column joints strengthened using CFRP composites", *Compos. Part B Eng*., **41**(1), 76-85. https://doi.org/10.1016/j.compositesb.2009.06.005.

Lee, J. and Fenves, G.L. (1998), "Plastic-damage model for cyclic loading of concrete structures", *J. Eng. Mech*., **124**(8), 892-900. https://doi.org/10.1061/(ASCE)0733-9399(1998)124:8(892).

Li, B. and Kulkarni, S.A. (2010), "Seismic behavior of reinforced concrete exterior wide beam-column joints", *J. Struct. Eng.,* **136**(1), 26-36. https://doi.org/10.1061/(ASCE)0733-9445(2010)136:1(26).

Liang, X. and Lu, T. (2018), "Seismic evaluation of engineered cementitious composites beam-column-slab subassemblies with various column-to-beam flexural strength ratios", *Struct. Concrete*, **19**(3), 735-746. https://doi.org/10.1002/suco.201600119.

Lu, X., Urukap, T.H., Li, S. and Lin, F. (2012), "Seismic behavior of interior RC beam-column joints with additional bars under cyclic loading", *Earthq. Struct.*, **3**(1), 37-57. https://doi.org/10.12989/eas.2012.3.1.037.

Lubliner, J., Oliver, J., Oller, S. and Oñate, E. (1989), "A plastic-damage model for concrete", *Int. J. Solid. Struct*., **25**(3), 299-326. https://doi.org/10.1016/0020-7683(89)90050-4.

McCormac, J.C. and Brown, R.H. (2015), *Design of Reinforced Concrete*, John Wiley & Sons.

Mobin, J.S., Kazemi, M.T. and Attari, N.K.A. (2016), "Cyclic behaviour of interior reinforced concrete beam-column connection with self-consolidating concrete", *Struct. Concrete*. **17**(4), 618-629. https://doi.org/10.1002/suco.201500133.

Niroomandi, A., Maheri, A., Maheri, M.R. and Mahini, S.S. (2010), "Seismic performance of ordinary RC frames retrofitted at joints by FRP sheets", *Eng. Struct*., **32**(8), 2326-2336. https://doi.org/10.1016/j.engstruct.2010.04.008.

Pampanin, S., Calvi, G.M. and Moratti, M. (2002), "Seismic behavior of RC beam-column joints designed for gravity only", *12th Eur. Conf. Earthq. Eng*.

Priestley, M.J.N. (1997), "Displacement-based seismic assessment of reinforced concrete buildings", *J. Earthq. Eng.*, **1**(1), 157-192. https://doi.org/10.1080/13632469708962365.

Ravi, R.S. and Arulraj, P.G. (2010), "Experimental investigation on behavior of reinforced concrete beam column joints retrofitted with GFRP-AFRP hybrid wrapping", *Int. J. Civil Struct. Eng.*, **1**(2), 245.

Realfonzo, R. and Napoli, A. (2009), "Cyclic behavior of RC columns strengthened by FRP and steel devices", *J. Struct. Eng*., **135**(10), 1164-1176. https://doi.org/10.1061/(ASCE)ST.1943-541X.0000048.

Roth, M.J., Slawson, T.R. and Flores, O.G. (2010), "Flexural and tensile properties of a glass fiber-reinforced ultra-high-strength concrete: an experimental, micromechanical and numerical study", *Comput. Concrete*, **7**(2), 169-190. https://doi.org/10.12989/cac.2010.7.2.169.

Saatcioglu, M., Mitchell, D., Tinawi, R., Gardner, N.J., Gillies, A.G., Ghobarah, A., Anderson, D.L. and Lau, D. (2001), "The August 17, 1999, Kocaeli (Turkey) earthquake-damage to structures", *Can. J. Civil Eng*., **28**(4), 715-737. https://doi.org/10.1139/cjce-28-4-715.

Sasmal, S., Ramanjaneyulu, K., Novák, B., Srinivas, V., Saravana Kumar, K., Korkowski, C., Roehm, C., Lakshmanan, N. and Iyer, N.R. (2011), "Seismic retrofitting of nonductile beam-column sub-assemblage using FRP wrapping and steel plate jacketing", *Constr. Build. Mater*., **25**(1), 175-182. https://doi.org/10.1016/j.conbuildmat.2010.06.041.

Sika Construction Chemicals (2006), Sikadur ® -30 LP, Product Data Sheet.

Supaviriyakit, T., Pimanmas, A. and Warnitchai, P. (2008), "Nonlinear finite element analysis of non-seismically detailed interior reinforced concrete beam-column connection under reversed cyclic load", *ScienceAsia*, **34**, 49-58. https://doi.org/10.2306/scienceasia1513-1874.2008.34.049.

Thirumalaiselvi, A., Anandavalli, N., Rajasankar, J. and Iyer, N.R. (2016), "Numerical evaluation of deformation capacity of laced steel-concrete composite beams under monotonic loading", *Steel Compos. Struct*., **20**(1), 167-184. http://dx.doi.org/10.12989/scs.2016.20.1.167.

Tsonos, A.D.G. (2014), "A new method for earthquake strengthening of old R/C structures without the use of conventional reinforcement", *Struct. Eng. Mech*., **52**(2), 391-403. http://dx.doi.org/10.12989/sem.2014.52.2.391.

Tsonos, A.G. (2004a), "Effectiveness of CFRP-jackets and RC-jackets in post-earthquake and pre-earthquake retrofitting of beam-column subassemblages", *13th World Conference on Earthquake Engineering*.

Tsonos, A.G. (2004b), "Improvement of the earthquake resistance of R/C beam-column joints under the influence of P-Δ effect and axial force variations using inclined bars", *Struct. Eng. Mech*., **18**(4), 389-410. https://doi.org/10.12989/sem.2004.18.4.389.

AT